Experimental and theoretical investigation of the stability of the monoclinic $BaWO_4$-II phase at high pressure and high temperature

R. Lacomba-Perales,[1,*] D. Martinez-García,[1] D. Errandonea,[1,2] Y. Le Godec,[3] J. Philippe,[3] G. Le Marchand,[3] J. C. Chervin,[3] A. Polian,[3] A. Múñoz,[4] and J. López-Solano[4]

[1]*MALTA Consolider Team, Departamento de Física Aplicada–ICMUV, Universitat de València, Edificio de Investigación, c/Dr. Moliner 50, 46100 Burjassot, Valencia, Spain*

[2]*Fundación General de la Universitat de València, Edificio de Investigación, c/Dr. Moliner 50, 46100 Burjassot, Valencia, Spain*

[3]*Institut de Minéralogie et de Physique des Milieux Condensés, Université Pierre et Marie Curie-Paris 6, CNRS UMR 7590, 140 rue de Lourmel, F-75015 Paris, France*

[4]*MALTA Consolider Team, Departamento de Física Fundamental II, and Instituto de Materiales y Nanotecnología, Universidad de La Laguna, E-38205 Tenerife, Spain*

(Received 22 February 2010; revised manuscript received 23 March 2010; published 16 April 2010)

In this work we report high-pressure (HP) and high-temperature (HT) *ex situ* and *in situ* experiments in $BaWO_4$. Starting from powder samples of $BaWO_4$, scheelite structure ($I4_1/a$), we reached conditions of 2.5–5.5 GPa and 400–1100 K using a Paris-Edinburgh press. The quenched samples were characterized by x-ray diffraction and Raman measurements at ambient conditions. Depending upon the final *P-T* conditions we found either the scheelite or the monoclinic $BaWO_4$-II ($P2_1/n$) structure. We also performed HP-HT *in situ* Raman measurements in a single crystal of $BaWO_4$ using a resistive-heated diamond-anvil cell. The transition from scheelite to the $BaWO_4$-II phase was observed at 5 GPa for $T=621$ K. *Ab initio* lattice-dynamics calculations have been performed in order to characterize the vibrations of the $BaWO_4$-II phase. Finally we carried out *in situ* powder angle-dispersive x-ray diffraction synchrotron measurements on $BaWO_4$ compound following different *P-T* paths, extending its measured phase diagram in the 2–6 GPa and 300–2000 K range.

DOI: 10.1103/PhysRevB.81.144117 PACS number(s): 62.50.−p, 64.70.kg, 63.20.D−, 61.05.cp

I. INTRODUCTION

Barium tungstate ($BaWO_4$) crystallizes at ambient conditions in the tetragonal scheelite structure [space group (SG) $I4_1/a$, No. 88, $Z=4$]. In this structure the W^{6+} cations are surrounded by four O^{2-} anions in a tetrahedral configuration, whereas the Ba^{2+} cations have eight oxygen ions nearest neighbors in a pseudocubic configuration.[1] This material has attracted the attention of crystals growers due to its excellent scintillating efficiency. In fact it has been shown to be an excellent laser-host material[2] and has been used in the construction of scintillating detectors.[3] Moreover from the fundamental point of view $BaWO_4$ presents remarkable features. The high-pressure (HP) and high-temperature (HT) phase diagram of $BaWO_4$ has been characterized by the *ex situ* experiments of Fujita *et al.*[4] This work reveals the appearance of either the scheelite or the monoclinic $BaWO_4$-II phase (SG $P2_1/n$, No. 14, $Z=8$), in the samples quenched from HP-HT depending on the *P-T* path followed in the experiments. The monoclinic phase has no direct resemblance with scheelite. It consists of WO_6 octahedra connected by edge and corner to irregular BaO_{12} polyhedra. The coordination number of the tungsten atoms increases from four to six and that of the barium atoms increases from eight to 12 in comparison with scheelite.[5] In addition in Ref. 4 an *ex situ* phase boundary between both structures is reported, P (GPa)$=2.67+0.00265$ T (°C); $T=600-1000$ °C. Recently, the structural stability of $BaWO_4$ was studied upon compression at room temperature (RT).[6,7] In these works two pressure-induced phase transitions are reported at 7 and 10 GPa involving monoclinic phases. In particular, Ref. 6 assigned the *M*-fergusonite structure (SG $I2/a$, No. 13, $Z=4$) to the first high-pressure phase and a $BaWO_4$-II-type phase to the one found beyond 10 GPa. In addition, *ab initio* calculations[6] clearly show that for $P>5$ GPa the energetically most favorable structure is the $BaWO_4$-II-type one. Also they noted that the *M*-fergusonite phase would be more stable than scheelite beyond 7.5 GPa. Recently, we made *in situ* angle-dispersive x-ray diffraction (ADXRD) synchrotron measurements in $BaWO_4$ at 7.5 GPa and up to 800 K.[8] We concluded that beyond 7 GPa a coexistence of scheelite and fergusonite is present at both RT and HT with no trace of the $BaWO_4$-II phase. From this and previous results we established a polymorphism zone in the *P-T* phase diagram in the range of 4–12 GPa and 300–800 K. The fact that different crystallographic structures are found at the same *P-T* conditions depending on the methods used in the studies, pointed out to the existence of kinetic barriers and possible nonhydrostatic experimental conditions.

Additional studies are needed to better understand the *P-T* phase diagram of $BaWO_4$. In particular there is a lack of *in situ* measurements in the 0–6 GPa; 300–1300 K range. These measurements are essential to characterize properly the HP-HT $BaWO_4$ phase diagram, to analyze *in situ* the transition from scheelite to the $BaWO_4$-II phase, and to test the *ex situ* phase boundary reported by Fujita *et al.*[4] With the motivation of understanding the nature of the $BaWO_4$-II phase, we present in this paper both *ex situ* and *in situ* studies using different experimental techniques. The *ex situ* measurements consisted of x-ray and Raman experiments on powder samples quenched from different *P-T* conditions (2.5–5.5 GPa and 400–1100 K), which have been obtained by means of a Paris-Edinburgh press. On the other hand we performed an *in situ* HP-HT Raman experiment on a single crystal of $BaWO_4$ in a diamond-anvil cell (DAC) at 5 GPa up to 621 K. *Ab initio* lattice-dynamics calculations have been per-

formed in order to characterize the vibrations of the phase II. Finally we have performed *in situ* ADXRD synchrotron measurements on powder samples for different *P-T* paths covering the range: 2–6 GPa and 300–2000 K. Thermal expansion coefficients are reported for both scheelite and $BaWO_4$-II structures for different values of pressure.

II. EXPERIMENTAL AND THEORETICAL DETAILS

The $BaWO_4$ samples used in our experiments consisted of either single crystals grown by the Czochralski method[9] or fine grained powder obtained from Alfa Aesar (99.9% purity). Several experimental *in situ* and *ex situ* techniques have been used in this work to characterize the HP-HT phase diagram of $BaWO_4$. Starting from powder samples, a Paris-Edinburgh press[10] has allowed us to reach different *P-T* experimental conditions. In the case of the *ex situ* experiments we first reached the desired pressure, then (under constant load) we increased slowly the temperature up to the one we wanted by means of a step by step current source. Finally, once we got the *P-T* final conditions required, we waited for stabilization 10 min, afterwards the current source was disconnected and the load in the press removed smoothly up to ambient conditions. Pressure and temperature were determined, respectively, by load-applied and power-temperature calibration curves[11] with experimental error less than 5%. The samples quenched to ambient conditions were characterized *ex situ* by x-ray diffraction measurements, using a Panalytical X'Pert Pro x-ray diffractometer working with the Cu wavelengths: $K_{\alpha 1}=1.5405$ Å and $K_{\alpha 2}=1.5444$ Å. Indexation and analysis of the structure were done using POWDERCELL.[12] Furthermore, we also performed Raman experiments on the quenched samples in the backscattering geometry using the 514.5 nm (2.41 eV) line of an Ar^+-ion laser with a power of less than 100 mW before the sample to avoid sample heating. A Mitutoyo 20× long working distance objective was used for focusing the laser on the sample and for collecting the Raman spectra. The scattered light was analyzed with a Jobin-Yvon T64000 triple spectrometer equipped with a confocal microscope in combination with a liquid-nitrogen-cooled multichannel charge-coupled-device detector. The spectral resolution was better than 1 cm^{-1}. Using the Paris-Edinburgh press, we have also performed *in situ* ADXRD synchrotron measurements at the ID 27 beamline of the ESRF (Grenoble, France). Experimental details could be found in Ref. 13. In this case the pressure was determined from the equation of state (EOS) of h-BN (Ref. 14) and the temperature was obtained from the mentioned power-temperature calibration curves. Monochromatic synchrotron radiation at $\lambda=0.3738$ Å was used for data collection. The size of the x-ray beam was focused and collimated down to 50×50 μm. A multichannel collimator (Soller slits) was used to isolate the diffraction signal of the sample from the surrounding environment. The diffraction images were integrated and corrected for distortions using FIT2D (Ref. 15) to yield intensity versus 2θ diagrams. Again, structure analysis was performed using POWDERCELL.[12] Finally, we used a 380 μm culet DAC with external an internal resistive heating[16] in order to perform an in *situ* HP-HT Raman experiment. The $BaWO_4$ sample consisted of a $20\times20\times5$ μm^3 not oriented single crystal. It was placed together with a ruby chip and a little piece of $SrB_4O_7:Sm^{2+}$ in a 125 μm hole of a rhenium gasket. As pressure-transmitting medium we used argon. The temperature was measured directly from a thermocouple placed in the internal furnace with a precision of ±1 K. However due to the existence of a temperature gradient the sample temperature is estimated to be 5 K smaller to that determined with the thermocouple.[17] The pressure was obtained by the $^7D_0-{}^5F_0$ fluorescence of $SrB_4O_7:Sm^{2+}$.[18] We also followed the R_1 line of the ruby[19] as a guide.

Lattice-dynamics calculations were performed within a standard first-principles scheme based on the density-functional theory and the pseudopotential method, as implemented in the Vienna *ab initio* simulation package (VASP) (see Ref. 20). The local-density approximation was adopted for the exchange and correlation potential. Projector-augmented wave[21,22] pseudopotentials were used and the semicore 5*p* electrons of W were treated explicitly as valence states. A kinetic-energy cutoff of 530 eV was used for the plane waves included in the basis set. The Monkhorst-Pack[23] method for integrations in the reciprocal space was used with dense grids appropriate to each structure. With these parameters, highly converged total energies of at least 1 meV per formula unit were obtained. At each selected volume, the structures were fully relaxed to their equilibrium configuration through the calculation of the forces on atoms, and the stress tensor.[24] In the relaxed equilibrium configuration, the forces were less than 0.001 eV/Å and the deviation of the stress tensor from a diagonal hydrostatic form was less than 0.1 GPa. These highly converged forces are required for the calculation of the phonon spectra at the Γ point using the direct force constant approach, or supercell method, as implemented in the PHONON program.[25,26] In this method, the dynamical matrix is obtained from the calculation of the forces over all atoms when each one individually is displaced from its equilibrium configuration. Only the atoms in the primitive cell have to be considered for the Γ point and crystal symmetry may further reduce the computational cost by identifying the independent distortions. Diagonalization of the dynamical matrix then provides both the frequencies of the normal modes and their polarization vectors, and allows the identification of the irreducible representation and character of the phonon modes. Note that the $BaWO_4$-II structure is centrosymmetric with $Z=8$. The vibrational modes have the following mechanical representation at Γ:[27] $\Gamma=36A_g+36A_u+36B_g+36B_u$, with 72 Raman active ($g$) modes and 72 IR active (u) modes, of which one A_u and two B_u are zero-frequency acoustic modes.

III. RESULTS AND DISCUSSIONS

A. *Ex situ* x-ray and Raman experiments

The aim of these experiments was to extend the *ex situ* study of Fujita *et al.*[4] and to present an experimental Raman characterization of the $BaWO_4$-II phase. For these purposes we reached different *P-T* experimental conditions in the range of 2.5–5.5 GPa and 400–1100 K. Our experiments re-

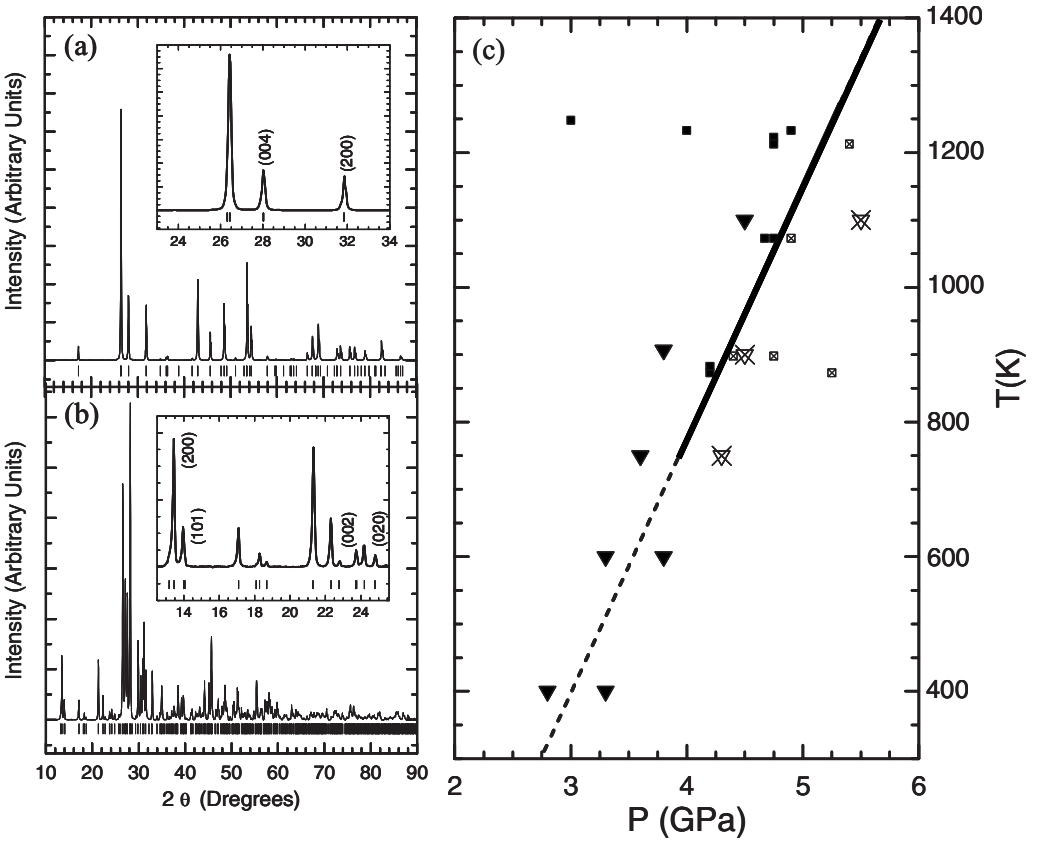

FIG. 1. Typical x-ray diffraction patterns obtained from the samples quenched to ambient conditions from the *ex situ* experiments, recovering either the (a) scheelite or (b) the $BaWO_4$-II structures. Also we present the *ex situ P-T* phase diagram of the $BaWO_4$ compound (c) in the range we performed the study. Inverted triangles: present work; small squares, Ref. 4. In both cases solid symbols correspond to the scheelite phase and open crossed symbols with the $BaWO_4$-II phase. The solid line corresponds to the *ex situ* equilibrium curve and the dashed one is its extrapolation.

veal that the samples quenched to ambient conditions have either the scheelite or the $BaWO_4$-II structure. In Figs. 1(a) and 1(b) we present the typical x-ray diffraction patterns obtained. In all cases we identify only one predominant phase for every quenched sample. The lattice parameters for each structure are presented in Table I, being in good agreement with previous works.[4,5] We also summarize in Fig. 1(c) the *ex situ P-T* phase diagram of $BaWO_4$ in the zone of interest. Basically we have followed the *ex situ* equilibrium curve reported by Fujita *et al.*[4] performing experiments in an extended *P-T* range. As it can be seen our results are in perfect agreement with the previous ones beyond 750 K.[4] However, up to 600 K we have just recovered the scheelite phase. Further on, in this paper, we will see that this fact supports the idea of the existence of kinetic barriers, which just make possible the appearance of the $BaWO_4$-II for particular values of pressure and temperature.[6]

Figure 2 presents the collected Raman spectra. For scheelite we observed 13 Raman actives modes, in agreement with previous works.[27] In Table II we report our experimental results compared with previous studies. In the case of $BaWO_4$-II phase we have performed lattice-dynamical calculations at ambient conditions. They reveal the existence of groups of modes quite close to each other with a total number of Raman active modes of 72. Experimentally we are able to assign 39 Raman-active modes to the various groups of neighboring modes. In Table III we associate each experimental mode with a theoretical or group of theoretical modes. The experimental and theoretical results are in fairly good agreement. For completion in the appendices we in-

TABLE I. Lattice parameters and volume of the samples quenched to ambient conditions from the Paris-Edinburgh experiments, which presented either scheelite or $BaWO_4$-II structure. In the second column are presented data from previous works.

Scheelite ($I4_1/a$)	
a=5.616 Å [a]	a=5.61 Å [b]
c=12.728 Å [a]	c=12.71 Å [b]
V=401.434 Å^3 [a]	V=400.01 Å^3 [b]
$BaWO_4$-II ($P2_1/n$)	
a=13.185 Å [a]	a=13.159 Å [c]
b=7.175 Å [a]	b=7.161 Å [c]
c=7.514 Å [a]	c=7.499 Å [c]
β=93.76° [a]	β=93.76° [c]
V=709.358 Å^3 [a]	V=705.122 Å^3 [c]

[a]Present work.
[b]Reference 7.
[c]References 4 and 5.

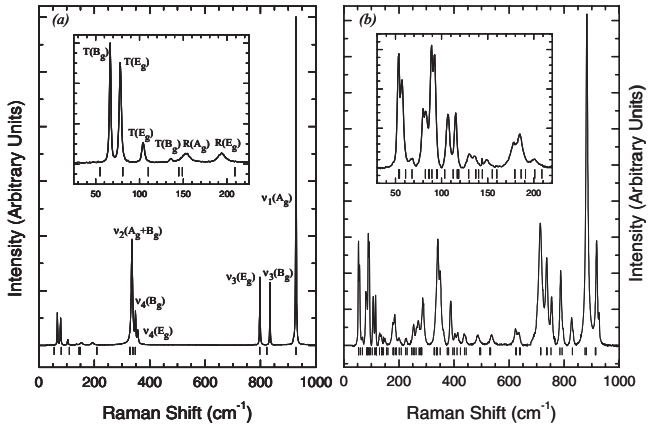

FIG. 2. Regular Raman spectra obtained from the quenched samples to ambient conditions, recovering either (a) the scheelite or (b) the $BaWO_4$-II structures. The ticks indicate the calculated positions for the Raman active phonons.

clude the calculated Raman and IR modes of $BaWO_4$-II and their pressure coefficients. If we compare the scheelite and the $BaWO_4$-II Raman spectra, first we note that in both cases the lowest mode appears beyond 50 cm^{-1}. Moreover, besides the much larger number of vibrations in phase II compared to scheelite, we would like to highlight that the absence of modes in the $\sim$360–800 cm^{-1} range found in the scheelite spectrum is not observed in the $BaWO_4$-II one. Another characteristic difference between the Raman spectra of the two structures is that the most intense peak in phase II is located at 882 cm^{-1} followed by a less intense one at 918 cm^{-1}, and at 928 cm^{-1} for the scheelite. This relative 46 cm^{-1} shift between the most intense peaks of each structure could be useful in order to discriminate them in an *in situ* experiment.

Recently, Tan *et al.*[28] reported the Raman spectrum of $BaWO_4$-II at ambient conditions. This spectrum is similar to that plotted in Fig. 2(b), however, due to experimental limitations, there are no Raman modes below 100 cm^{-1}. These authors also showed that quenched $BaWO_4$-II remains stable at RT up to 14.8 GPa. Despite the similitude between their Raman spectra with those here and in Ref. 27 assigned to $BaWO_4$-II, they claimed that the HP phase previously observed at RT beyond 10 GPa (Ref. 6) could not be the $BaWO_4$-II one. This conclusion is contradicted by our experiments. In Fig. 3 we show a Raman spectrum of a single crystal of $BaWO_4$ taken at RT and 7.6 GPa in a DAC using neon as pressure-transmitting medium and a spectrum of $BaWO_4$-II at ambient conditions. Although the peaks broaden, there are appreciable similarities between the spectra. Similar features can be seen in the Raman spectrum measured by Manjon *et al.* at 9 GPa,[27] where 41 Raman modes were identified and assigned to a $BaWO_4$-II-type phase. Clearly in both spectra there are similar modes below 100 cm^{-1}. Also we remark the group of modes in the range from 200 to 450 cm^{-1}; in the case of the spectrum at RT and 7.6 GPa the modes overlap probably due to the effect of pressure. We can also see peaks at 500 cm^{-1} and an absence of them from 550 to 600 cm^{-1}. Finally, beyond 600 cm^{-1} we can nearly identify all the groups of peaks noting the intense mode at 900 cm^{-1} and the less intense one immediately subsequent. In view of these comments we think there

TABLE II. Summary of the Raman results in scheelite $BaWO_4$. The first two columns correspond to previous theoretical calculations and experimental data at ambient conditions. The third column are the modes from our *ex situ* studies of the quenched samples to ambient conditions which presented the scheelite structure. In the last column we present the *in situ* modes of the scheelite at 5 GPa and RT as well as the slope of their temperature dependence. We could neither find nor follow the $R(E_g)$ in our measurements.

	Previous[a]				
	Theory	Experiment	Experiment (*Ex situ*)	Experiment (*In situ*)	
	$\omega(cm^{-1})$ $P=0$; $T=293$ K		$\omega(cm^{-1})$ $P=0$; $T=293$ K	$\omega(cm^{-1})$ $P=5$ GPa ; $T=293$ K	$(\partial\omega/\partial T)_{5\ GPa}$ (cm^{-1}/mK)
$T(B_g)$	55	63	67	59	-7 ± 3
$T(E_g)$	81	74	78	78	-19 ± 2
$T(E_g)$	110	101	104	116	-16 ± 2
$T(B_g)$	145	133	136	157	-20 ± 6
$R(A_g)$	149	150	153	170	-32 ± 3
$R(E_g)$	209	191	194		
$\nu_2(A_g)$	328	331	336	347	-9 ± 3
$\nu_2(B_g)$	329	332	336	347	-9 ± 3
$\nu_4(B_g)$	339	344	348	347	-9 ± 3
$\nu_4(E_g)$	348	352	357	368	-9 ± 4
$\nu_3(E_g)$	797	795	798	811	-11 ± 2
$\nu_3(B_g)$	823	831	834	842	-7 ± 3
$\nu_1(A_g)$	928	926	928	940	-9 ± 2

[a]Reference 11.

TABLE III. Theoretical and experimental Raman active modes of the $BaWO_4$-II structure at ambient conditions. The experimental modes are obtained directly from the spectrum in Fig. 2(b) and assigned to one theoretical or group of theoretical modes.

Mode (sym)	ω teo (cm^{-1})	ω exp (cm^{-1})	Mode (sym)	ω teo (cm^{-1})	ω exp (cm^{-1})	Mode (sym)	ω teo (cm^{-1})	ω exp (cm^{-1})	Mode (sym)	ω teo (cm^{-1})	ω exp (cm^{-1})
A_g	53.4	53	A_g	140.2	149	B_g	280.9	288	A_g	529.9	536
B_g	54.4		B_g	144.2		A_g	283.1		B_g	533.0	
A_g	60.9	57	B_g	155.0	160	A_g	327.5	334	A_g	624.8	624
B_g	67.9	68	A_g	159.9		B_g	329.7		B_g	626.0	
A_g	82.4	80	A_g	179.1	178	A_g	336.5	341	A_g	638.8	636
B_g	86.2	83	B_g	179.5		B_g	338.3		B_g	639.9	
A_g	86.7		A_g	186.2	185	A_g	338.8		B_g	714.1	713
A_g	89.5	89	B_g	190.9		B_g	349.7	350	A_g	715.3	
B_g	94.6	92	B_g	201.0	201	B_g	375.7	388	B_g	736.0	736
B_g	95.3		A_g	208.7		A_g	380.3		A_g	738.0	
A_g	103.3	107	A_g	224.1	226	A_g	395.7	403	A_g	752.0	754
A_g	112.5	115	B_g	229.9		B_g	400.9		B_g	784.4	787
B_g	116.9		B_g	246.1	253	A_g	411.2	414	A_g	792.0	
A_g	117.6		A_g	250.9		B_g	423.1		B_g	829.6	827
B_g	118.4		B_g	255.5		B_g	438.1	439	A_g	875.6	882
B_g	129.3	130	A_g	262.0	265	A_g	444.0		B_g	880.8	
B_g	136.8	136	A_g	273.1	270	A_g	492.9	486	B_g	913.0	918
A_g	137.1		B_g	276.7		B_g	496.6		A_g	914.8	

is enough evidence to support that the RT-HP phase has a $BaWO_4$-II-type structure. This hypothesis is consistent also with *ab initio* calculations,[6] optical absorption,[29] x-ray diffraction,[30] and Raman measurements.[27]

B. *In situ* Raman experiment

Once we had a characterization of the Raman modes for the $BaWO_4$-II phase, our next objective has been to analyze *in situ* the phase transition from the scheelite to the $BaWO_4$-II structure by means of HP-HT Raman spectroscopy. In Fig. 4 we present a summary of the collected Raman spectra. In this experiment the pressure was first increased up to 5 GPa at RT. Then the temperature was increased keeping the pressure constant at 5 GPa. As we show in Fig. 5, most of the scheelite Raman active modes can be followed up to 571 K. In Table II we sum up the modes of the scheelite at 5 GPa

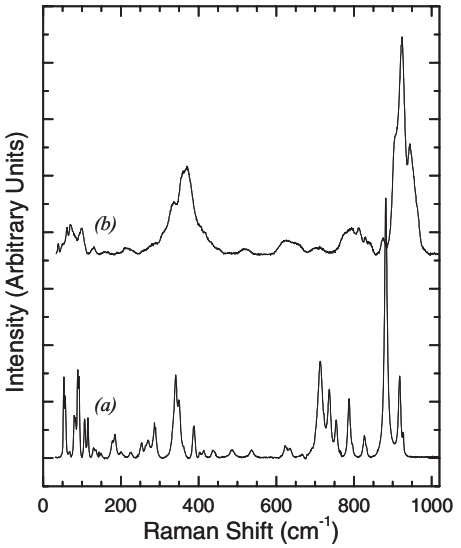

FIG. 3. Raman spectra of: (a) $BaWO_4$-II phase at ambient conditions and (b) single crystal of $BaWO_4$ at 7.6 GPa with neon as pressure-transmission medium. The similarities found in both spectra could confirm that the RT-HP phase of the $BaWO_4$ compound is the monoclinic $BaWO_4$-II structure.

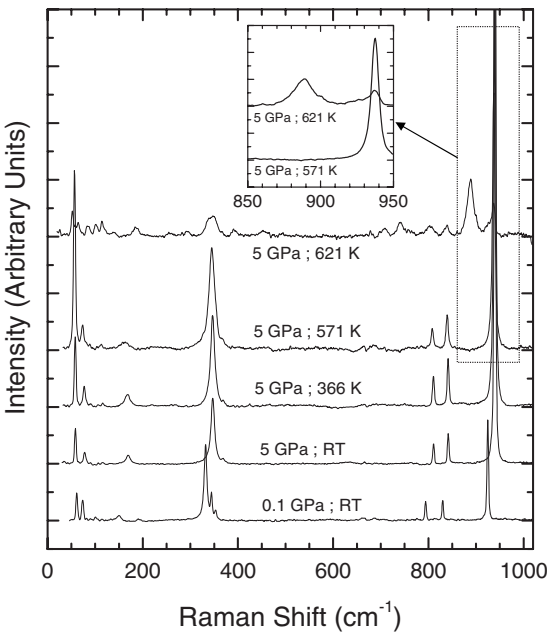

FIG. 4. *In situ* Raman spectra at HP and HT for a single crystal of $BaWO_4$. Changes in the spectra are found at 5 GPa and 621 K.

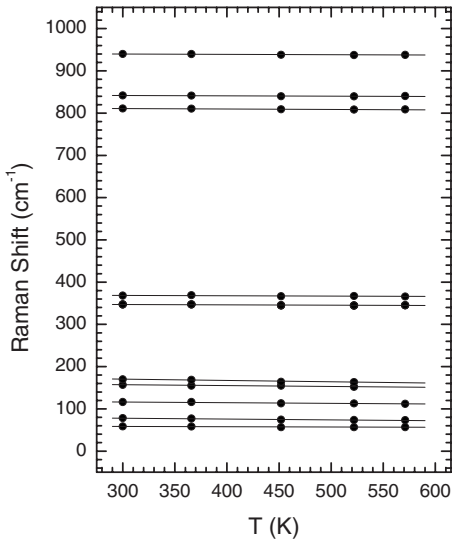

FIG. 5. Temperature dependence of the Raman-active modes for the scheelite structure in $BaWO_4$ at 5 GPa.

and RT and their temperature coefficients for that pressure that are all negative. At 5 GPa and 621 K dramatic changes appear in the Raman spectrum (Fig. 4). Peaks appear both at low and high frequency, and the most intense peak is placed at 889 cm^{-1} instead of 938 cm^{-1} at lower temperature (see the inset in Fig. 4). Figure 6 shows pictures of the pressurized sample: up to 571 K the sample is transparent and compact, at 621 K it becomes opaque and several defects appear on it. Yet it is not clear if the nature of these defects is related to the kinetics of the transition or to a nucleation and growth process. This evidence points out that a phase transition took place. In order to confirm that the new phase corresponds to the $BaWO_4$-II one, Fig. 7 shows both the *ex situ* Raman spectrum at ambient conditions and the *in situ* one obtained at 5 GPa and 621 K. The resemblance between both spectra is evident. So, we can conclude that we have seen *in situ* the phase transition from the scheelite to the $BaWO_4$-II structure. At that point, we quenched the sample to ambient conditions and we recovered the scheelite structure. This result

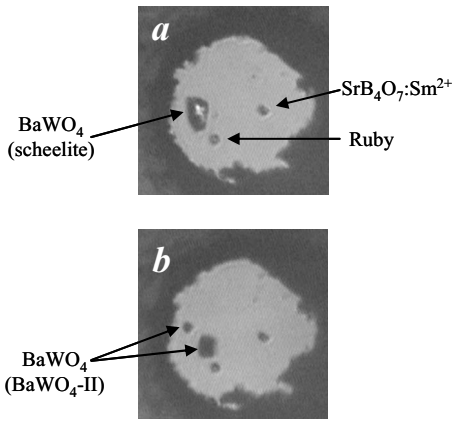

FIG. 6. Pictures corresponding to the HP-HT Raman measurement in the DAC, (a) before the transition (5 GPa and 522 K) and (b) after the transition (5 GPa and 621 K) where the appearance of defects opacifies the sample.

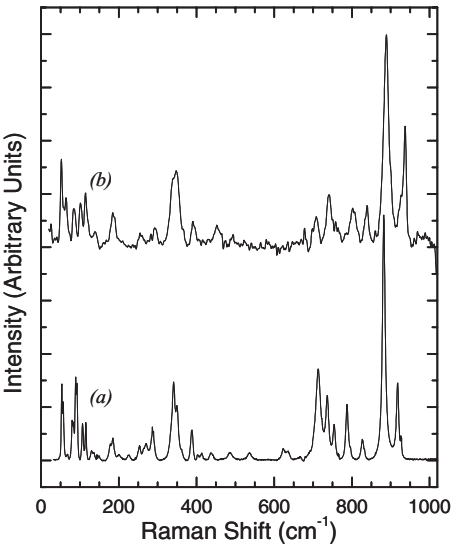

FIG. 7. Comparison of the Raman spectrum of $BaWO_4$ II at ambient conditions with the Raman spectrum of $BaWO_4$ compound at (a) 5.0 GPa and (b) 621 K. The similar features prove the occurrence of the phase transition from the scheelite to the $BaWO_4$-II structure.

is in agreement with our *ex situ* measurements.

C. *In situ* ADXRD synchrotron experiments

We have performed *in situ* ADXRD synchrotron measurements at the ID 27 beamline (ESRF) using a Paris-Edinburgh press. In a first step we increased the pressure up to 6 GPa at

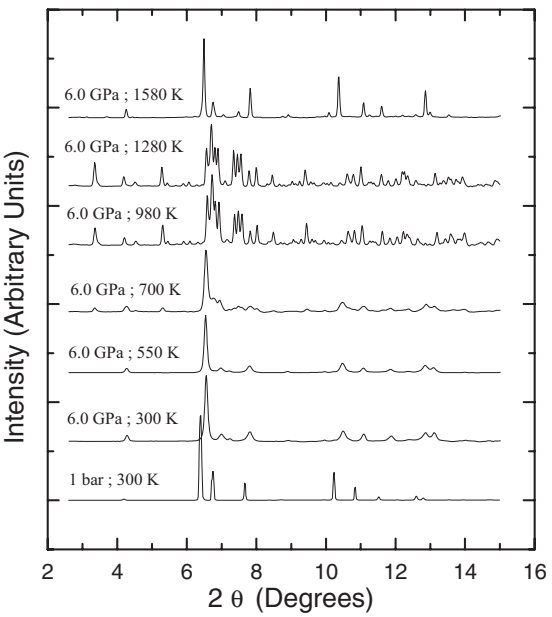

FIG. 8. Selected spectra from the *in situ* HP-HT synchrotron ADXRD experiments performed on $BaWO_4$ compound. Changes from the scheelite spectrum are observed at 6 GPa and 700 K. The new HP-HT phase which corresponds with the $BaWO_4$-II structure is completed at 6 GPa and 980 K. Further temperature increase induces the back transformation to the scheelite structure at 6 GPa and 1580 K.

TABLE IV. Experimental lattice parameters and cell volume for the monoclinic $BaWO_4$-II structure at 6 GPa for different temperatures. The last row corresponds to the experimental values at 10.9 GPa and RT reported in Ref. 6.

T (K)	**a** (Å)	**b** (Å)	**c** (Å)	β (deg)	**V** (Å^3)
700	12.803	7.002	7.395	92.578	662.247
770	12.794	7.020	7.398	92.272	663.911
980	12.757	7.040	7.401	92.331	664.087
1280	12.779	7.072	7.425	92.344	671.777
10.9 GPa and RT	12.841	7.076	7.407	93.0	672.100

RT. Then, at constant load, we raised the temperature up to 1580 K. In Fig. 8 we show a summary of the collected spectra. As it can be seen at 6 GPa changes in the spectra are found at 700 K. The emergent phase, which perfectly corresponds to the $BaWO_4$-II structure is completed at 980 K. At higher temperature, the $BaWO_4$-II structure is preserved up to 1280 K, and at 1580 K the scheelite phase reappears. Table IV presents the lattice parameters and cell volume for the $BaWO_4$-II phase at 6 GPa and different temperatures. At 6 GPa and 700 K, the volume reduction is 6% compared to the ambient conditions (see Table I). The last row of Table IV presents the experimental lattice parameters reported in Ref. 6 at 10.9 GPa and RT and show that the lattice parameters of the RT and HP phase are similar to the HT-HP ones. Figure 9 presents the temperature dependence of the unit-cell volume for the several situations described above. The high-pressure behavior of the scheelite phase at RT (up to 6 GPa) is in good agreement with previous results.[6] The phases I and II present a linear thermal volume expansion, whose value at 6 GPa is 2.5×10^{-5} K^{-1} for the scheelite structure and of 1.8×10^{-5} K^{-1} for the $BaWO_4$-II phase. The volume of the "re-entrant" scheelite at 6 GPa and 1580 K is on the extrapo-

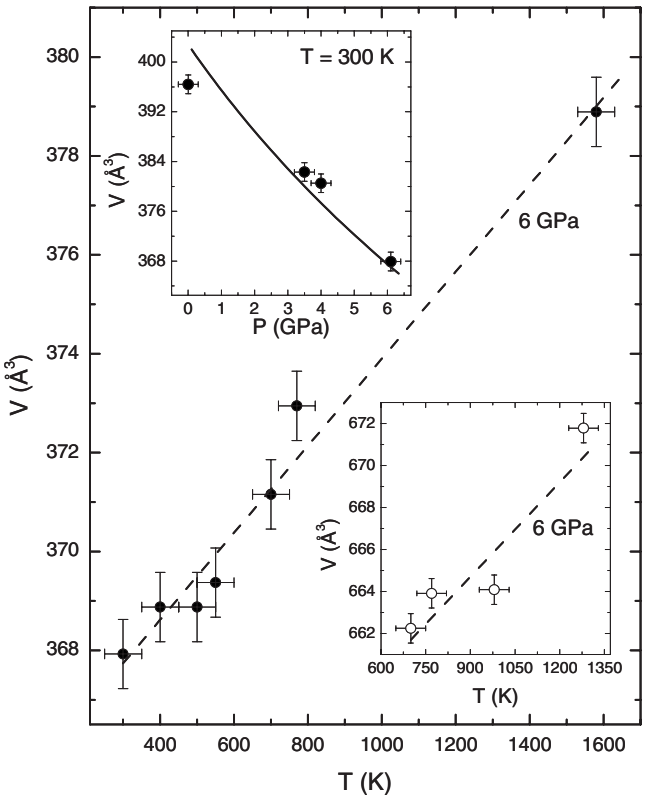

FIG. 9. Unit-cell volume of $BaWO_4$ as a function of temperature at 6 GPa. The solid symbols correspond to the scheelite structure and the open ones to the $BaWO_4$-II phase. The inset at the top-left corner shows the pressure dependence of the scheelite structure at RT. The circles are the experimental data and the solid curve corresponds to the EOS reported in Ref. 6. The inset at the bottom-right corner shows the temperature dependence of the unit-cell volume of $BaWO_4$ II at 6 GPa. The dashed lines are linear fits to the HT data.

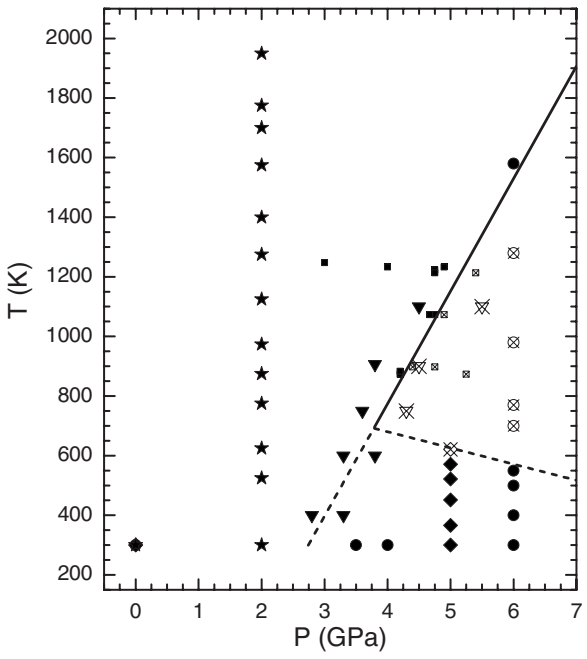

FIG. 10. Extended phase diagram for the $BaWO_4$ compound. Solid symbols correspond to the scheelite structure and open crossed ones to the $BaWO_4$-II phase. Various symbols represent the several experimental techniques used: small squares: data of Ref. 4; inverted triangles: *ex situ* x-ray and Raman measurements presented in Sec. III A; diamonds: *in situ* Raman data of Sec. III B; circles and stars: *in situ* ADXRD synchrotron experiments shown in Sec. III C. The straight line represents the phase boundary between the scheelite and the $BaWO_4$ II reported in Ref. 4 while the dashed lines are the kinetic barrier frontiers where the scheelite is metastable.

TABLE V. Theoretical Raman modes at 1 bar and their pressure coefficients.

Mode (sym)	ω (cm^{-1})	$d\omega/dP$ (cm^{-1}/GPa)	Mode (sym)	ω (cm^{-1})	$d\omega/dP$ (cm^{-1}/GPa)	Mode (sym)	ω (cm^{-1})	$d\omega/dP$ (cm^{-1}/GPa)	Mode (sym)	ω (cm^{-1})	$d\omega/dP$ (cm^{-1}/GPa)
A_g	53.4	1.04	A_g	140.2	3.14	B_g	280.9	2.71	A_g	529.9	1.30
B_g	54.4	1.89	B_g	144.2	2.24	A_g	283.1	1.98	B_g	533.0	1.40
A_g	60.9	2.38	B_g	155.0	3.44	A_g	327.5	–0.09	A_g	624.8	3.76
B_g	67.9	1.04	A_g	159.9	4.07	B_g	329.7	0.58	B_g	626.0	3.72
A_g	82.4	1.85	A_g	179.1	1.33	A_g	336.5	1.67	A_g	638.8	3.86
B_g	86.2	2.11	B_g	179.5	1.38	B_g	338.3	2.80	B_g	639.9	3.86
A_g	86.7	1.46	A_g	186.2	2.27	A_g	338.8	3.20	B_g	714.1	0.97
A_g	89.5	0.97	B_g	190.9	1.97	B_g	349.7	1.91	A_g	715.3	0.88
B_g	94.6	1.36	B_g	201.0	1.09	B_g	375.7	2.01	B_g	736.0	3.05
B_g	95.3	2.25	A_g	208.7	1.04	A_g	380.3	1.77	A_g	738.0	3.28
A_g	103.3	2.44	A_g	224.1	2.16	A_g	395.7	1.71	A_g	752.0	3.43
A_g	112.5	1.90	B_g	229.9	2.89	B_g	400.9	1.65	B_g	784.4	3.71
B_g	116.9	2.47	B_g	246.1	0.22	A_g	411.2	2.56	A_g	792.0	4.17
A_g	117.6	3.05	A_g	250.9	2.07	B_g	423.1	2.34	B_g	829.6	3.58
B_g	118.4	2.17	B_g	255.5	2.41	B_g	438.1	3.84	A_g	875.6	2.86
B_g	129.3	1.07	A_g	262.0	1.87	A_g	444.0	3.54	B_g	880.8	3.08
B_g	136.8	3.12	A_g	273.1	3.24	A_g	492.9	3.09	B_g	913.0	3.67
A_g	137.1	2.06	B_g	276.7	2.73	B_g	496.6	3.10	A_g	914.8	3.30

lation of the initial scheelite before the phase transition to the $BaWO_4$-II structure.

A second run was performed at 2 GPa vs temperature up to 1950 K. No phase transition was observed, the sample remaining in the scheelite structure for the whole studied range. In addition, $BaWO_4$ does present neither decomposition nor melting in the studied pressure-temperature range. Actually in the case of the scheelite phase we can establish an estimation of the lower limit for the melting temperature. According to Ref. 31 the melting point at ambient pressure for scheelite $BaWO_4$ is T_m=1775 K. At 2 GPa and 1950 K the sample is still solid in the scheelite structure. Hence,

TABLE VI. Theoretical IR modes at 1 bar and their pressure coefficients.

Mode (sym)	ω (cm^{-1})	$d\omega/dP$ (cm^{-1}/GPa)	Mode (sym)	ω (cm^{-1})	$d\omega/dP$ (cm^{-1}/GPa)	Mode (sym)	ω (cm^{-1})	$d\omega/dP$ (cm^{-1}/GPa)	Mode (sym)	ω (cm^{-1})	$d\omega/dP$ (cm^{-1}/GPa)
B_u	0.0		B_u	126.2	3.69	B_u	305.1	0.97	B_u	447.1	3.40
A_u	0.0		A_u	130.0	3.20	A_u	306.9	0.90	A_u	474.0	1.77
B_u	0.0		A_u	143.3	2.89	A_u	309.0	1.50	A_u	581.8	3.75
A_u	40.4	2.02	B_u	155.5	3.31	B_u	310.9	2.12	B_u	582.7	3.90
B_u	41.9	0.70	A_u	158.6	3.53	B_u	333.6	2.31	B_u	599.6	3.47
A_u	61.3	1.22	B_u	162.8	3.37	A_u	336.8	2.23	A_u	605.2	3.30
B_u	71.1	1.50	B_u	183.3	2.57	B_u	356.6	1.28	B_u	725.3	2.45
A_u	73.7	1.87	A_u	185.0	1.85	A_u	359.0	1.10	A_u	729.0	2.63
B_u	79.0	2.10	B_u	203.9	1.41	A_u	379.4	3.03	B_u	738.3	3.36
A_u	85.8	2.76	A_u	204.5	1.76	B_u	384.0	2.66	A_u	745.4	3.34
B_u	88.2	0.79	A_u	211.5	3.38	B_u	402.3	2.15	B_u	773.0	3.08
A_u	95.2	1.86	B_u	211.9	2.79	A_u	404.9	1.67	A_u	794.8	3.37
B_u	100.0	0.44	A_u	235.2	1.38	A_u	410.0	2.10	A_u	796.3	4.06
A_u	103.8	1.74	B_u	236.6	1.68	B_u	410.0	1.94	B_u	829.7	3.32
B_u	108.2	2.39	A_u	260.7	0.43	A_u	414.0	2.21	B_u	869.3	3.37
A_u	109.8	1.41	B_u	266.2	0.03	B_u	415.8	2.35	A_u	873.6	3.13
B_u	117.3	3.20	B_u	286.3	0.79	A_u	441.8	4.23	B_u	895.3	3.41
A_u	120.0	2.02	A_u	290.8	1.06	B_u	442.5	2.70	A_u	909.1	3.17

$\partial T_m/\partial P > 87$ K GPa^{-1}, a value similar to the low-pressure melt slopes of many lower mantle minerals.[32]

D. Extended phase diagram for $BaWO_4$ compound

Based upon previous results and our *ex situ* and *in situ* measurements, we present in Fig. 10 an extension of the phase diagram of $BaWO_4$. *Ab initio* calculations[6] estimated that beyond 5 GPa the most stable phase is the $BaWO_4$-II one. However, experimentally this phase was found above 11 GPa at RT.[6] In fact, before the appearance of $BaWO_4$ II, an *M*-fergusonite structure was observed around 7 GPa. A possible explanation for the discrepancy between the theoretical and experimental results is the existence of kinetic barriers, which inhibited the direct appearance of the $BaWO_4$-II phase.[6] Note that the scheelite-$BaWO_4$-II transition is a first-order transformation and the scheelite-fergusonite transition is a second-order transformation. The data presented in Fig. 10 confirm this hypothesis. The picture is as follows. The equilibrium curve with positive slope establishes the transition between the scheelite and the $BaWO_4$-II structure. The scheelite-$BaWO_4$-II equilibrium boundary at RT is around 3 GPa. However the scheelite structure remains at the right-hand side of this line and below the negative slope curve obtained thanks to our *in situ* measurements. This curve establishes the *P-T* kinetic-barrier frontier that should be crossed in order to obtain the $BaWO_4$-II phase. Actually its extrapolation for high pressures gives a value around 11 GPa at 300 K, just the pressure at which the $BaWO_4$-II was experimentally observed at RT.[6] Finally, the *in situ* ADXRD at 6 GPa and HT measurement which showed the reappearance of the scheelite above the equilibrium curve around 1600 K, confirm our explanation of the *P-T* phase diagram of $BaWO_4$.

IV. CONCLUSIONS

Our work confirms that $BaWO_4$ II is the stable HP and HT phase of $BaWO_4$. This phase has been found *in situ* under conditions of HP-HT by means of two different experimental techniques: Raman in a resistive-heating DAC and ADXRD synchrotron radiation experiments in a Paris-Edinburgh press. We also have performed *ex situ* experiments and lattice-dynamics calculations which have allowed us to better understand our *in situ* results. A *P-T* phase diagram in the range 0–6 GPa and 300–1950 K for $BaWO_4$ has been proposed. We found that the scheelite structure remains metastable at low *P-T* conditions where the $BaWO_4$-II phase should be stable, proving the hypothesis that the phase transition between scheelite and $BaWO_4$-II involves a complex mechanism and the existence of kinetics barriers. Furthermore we provide evidence supporting that $BaWO_4$-II is the structure obtained upon compression at RT. In addition the Raman modes of $BaWO_4$-II have been accurately studied. We have been able to establish a good agreement between our experiments at ambient conditions and the theoretical modes. On the other hand, we have also reported the HT evolution of the Raman active modes in the case of the scheelite phase at 5 GPa. As well we have established experimentally the volume thermal expansion of the scheelite and the $BaWO_4$-II structures at 6 GPa. Finally, just to say that in our experiments we have not found evidence of neither decomposition nor fusion of the sample.

ACKNOWLEDGMENTS

Financial support from Spanish Consolider Ingenio 2010 Program (Project No. CSD2007-00045) is acknowledged. This work was also supported by Spanish MICCIN (Grant No. MAT2007-65990-C03-01), and the French "Réseau Hautes Pressions" and "Mission Ressources et Compétences Technologiques" of the CNRS. High-pressure experiments at ESRF have been carried out during beam time allocated to proposal HS-2532 at beamline ID27. We are grateful to Jean-Philippe Perrillat for his help in the synchrotron x-ray diffraction measurements. R.L.-P. thanks the support of the MICINN through the FPU program.

APPENDIX

For completion in Table V and Table VI we present, respectively, the Raman active modes and the IR active modes at 1 bar as well as their pressure coefficients for the $BaWO_4$-II phase, obtained from our *ab initio* lattice-dynamics calculations.

*Corresponding author; raul.lacomba@uv.es

[1] A. W. Sleight, Acta Crystallogr., Sect. B: Struct. Crystallogr. Cryst. Chem. **28**, 2899 (1972).
[2] L. I. Ivleva, I. S. Voronina, P. A. Lykov, L. Yu. Berezovskaya, and V. V. Osito, J. Cryst. Growth **304**, 108 (2007).
[3] M. Bravin, M. Bruckmayer, C. Bucci, S. Cooper, S. Giordano, F. Von Feilitzsch, J. Hohne, J. Jochum, V. Jorgens, R. Keeling, H. Kraus, M. Loidl, J. Lush, J. Macallister, J. Marchese, O. Meier, P. Meunier, U. Nagel, T. Nussle, F. Probst, Y. Ramachers, H. Sarsa, J. Schnagl, W. Seidel, I. Sergeyev, M. Sisti, L. Stodolsky, S. Uchaikin, and L. Zerle, Astropart. Phys. **12**, 107 (1999).
[4] T. Fujita, S. Yamaoka, and O. Fukunaga, Mater. Res. Bull. **9**, 141 (1974).
[5] I. Kawada, K. Kato, and T. Fujita, Acta Crystallogr., Sect. B: Struct. Crystallogr. Cryst. Chem. **30**, 2069 (1974).
[6] D. Errandonea, J. Pellicer-Porres, F. J. Manjón, A. Segura, Ch. Ferrer-Roca, R. S. Kumar, O. Tschauner, J. López-Solano, P. Rodríguez-Hernández, S. Radescu, A. Mujica, A. Muñoz, and G. Aquilanti, Phys. Rev. B **73**, 224103 (2006).
[7] V. Panchal, N. Garg, A. K. Chauhan, Sangeeta, and S. M. Sharma, Solid State Commun. **130**, 203 (2004).
[8] R. Lacomba-Perales, D. Martínez-García, D. Errandonea, Y. Le Godec, J. Philippe, and G. Morard, High Press. Res. **29**, 76 (2009).

[9] W. Ge, H. Zhang, J. Wang, J. Liu, X. Xu, X. Hu, J. Li, and M. Jiang, J. Cryst. Growth **270**, 582 (2004).
[10] J. M. Besson, R. J. Nelmes, G. Hamel, J. S. Loveday, G. Weill, and S. Hull, Physica B **180-181**, 907 (1992).
[11] Y. Le Godec, Ph.D. thesis, University of Paris VII, 1999.
[12] W. Kraus and G. Nolze, J. Appl. Crystallogr. **29**, 301 (1996).
[13] Y. Le Godec, G. Hamel, J. Philippe, D. Martinez-Garcia, T. Hammouda, V. L. Solozhenko, W. Crichton, M. Mezouar, and S. Klotz, J. Synchrotron Radiat. **16**, 513 (2009).
[14] Y. Le Godec, D. Martínez-García, M. Mezouar, G. Syfosse, and J. P. Itié, High Press. Res. **17**, 35 (2000).
[15] A. P. Hammersley, ESRF Internal Report No. ESRF97HA02T, 1997 (unpublished); A. P. Hammersley, S. O. Svensson, M. Hanfland, A. N. Fitch, and D. Häusermann, High Press. Res. **14**, 235 (1996).
[16] J. C. Chervin, B. Canny, J. M. Besson, and Ph. Pruzan, Rev. Sci. Instrum. **66**, 2595 (1995).
[17] W. Montgomery, J. M. Zaug, W. M. Howard, A. F. Goncharov, J. C. Crowhurst, and R. Jeanloz, J. Phys. Chem. B **109**, 19443 (2005).
[18] F. Datchi, R. Le Toullec, and P. Loubeyre, J. Appl. Phys. **81**, 3333 (1997).
[19] H. K. Mao, J. Xu, and P. M. Bell, J. Geophys. Res. **91**, 4673 (1986).
[20] G. Kresse *et al.*, Computer code VASP, http://cms.mpi.univie.ac.at/vasp
[21] P. E. Blöchl, Phys. Rev. B **50**, 17953 (1994).
[22] G. Kresse and D. Joubert, Phys. Rev. B **59**, 1758 (1999).
[23] H. J. Monkhorst and J. D. Pack, Phys. Rev. B **13**, 5188 (1976).
[24] G. Kresse and J. Furthmüller, Phys. Rev. B **54**, 11169 (1996).
[25] G. Kresse, J. Furthmüller, and J. Hafner, Europhys. Lett. **32**, 729 (1995).
[26] K. Parlinski, Computer code PHONON, http://wolf.ifj.edu.pl/phonon
[27] F. J. Manjón, D. Errandonea, N. Garro, J. Pellicer-Porres, P. Rodríguez-Hernández, S. Radescu, J. López-Solano, A. Mujica, and A. Muñoz, Phys. Rev. B **74**, 144111 (2006).
[28] D.-Y. Tan, W.-S. Xiao, W.-G. Zhou, M.-S. Song, X.-L. Xiong, and M. Chen, Chin. Phys. Lett. **26**, 120502 (2009).
[29] R. Lacomba-Perales, D. Errandonea, D. Martínez-García, J.-C. Chervin, and A. Polian, 47th EHPRG International Conference, Paris (France), 6–11 September, 2009 (unpublished).
[30] D. Errandonea and F. J. Manjon, Prog. Mater. Sci. **53**, 711 (2008).
[31] W. W. Ge, H. J. Zhang, J. Y. Wang, J. H. Liu, X. G. Xu, X. B. Hu, and M. H. Jiang, J. Appl. Phys. **98**, 013542 (2005).
[32] G. Shen and P. Lazor, J. Geophys. Res. **100**, 17699 (1995).